JACS
JOURNAL OF THE AMERICAN CHEMICAL SOCIETY



Article

# Highly Active Gas Phase Organometallic Catalysis Supported Within Metal-organic Framework Pores

Ricardo A. Peralta, Michael T. Huxley, Jack D. Evans, Thomas Fallon, Haijie Cao, Maoxia He, Xiu Song Zhao, Stefano Agnoli, Christopher J. Sumby, and Christian J. Doonan

*J. Am. Chem. Soc.*, **Just Accepted Manuscript** • DOI: 10.1021/jacs.0c05286 • Publication Date (Web): 10 Jul 2020



## Just Accepted



is published by the American Chemical Society. 1155 Sixteenth Street N.W., Washington, DC 20036

# Highly Active Gas Phase Organometallic Catalysis Supported Within Metal-organic Framework Pores

Ricardo A. Peralta[a], Michael T. Huxley[a], Jack D. Evans[b], Thomas Fallon[a], Haijie Cao[c], Maoxia He[d], Xiu Song Zhao[c,e], Stefano Agnoli[f], Christopher J. Sumby[a]* and Christian J. Doonan[a]*

[a] Centre for Advanced Nanomaterials and Department of Chemistry, The University of Adelaide, North Terrace, Adelaide, SA 5000, Australia. Email: christopher.sumby@adelaide.edu.au (CJS); christian.doonan@adelaide.edu.au (CJD)

[b] Department of Inorganic Chemistry, Technische Universität Dresden, Bergstraße 66, 01062 Dresden, Germany

[c] Institute of Materials for Energy and Environment, College of Materials Science and Engineering, Qingdao University, Qingdao, 266071, PR China

[d] Environment Research Institute, Shandong University, Qingdao, 266237, PR China

[e] School of Chemical Engineering, The University of Queensland, St Lucia, Brisbane, 4072. Australia

[f] Dipartimento di Scienze Chimiche, Università di Padova, Via Marzolo 1, 35131 Padova, Italy

Catalysis, Heterogeneous Catalysts, Metal-organic Framework, Single Crystal X-ray Diffraction, Post-synthetic Metalation

**ABSTRACT:** Metal-organic Frameworks (MOFs) can act as a platform for the heterogenization of molecular catalysts, providing improved stability, allowing easy catalyst recovery and a route towards structural elucidation of the active catalyst. We have developed a MOF, **1**, possessing vacant *N,N*-chelating sites which are accessible via the porous channels that penetrate the structure. In the present work, cationic rhodium(I) norbornadiene (NBD) and bis(ethylene) (ETH) complexes paired with both non-coordinating and coordinating anions have been incorporated into the *N,N*-chelation sites of **1** via post-synthetic metalation and facile anion exchange. Exploiting the crystallinity of the host framework, the immobilized Rh(I) complexes were structurally characterized using X-ray crystallography. The ethylene hydrogenation catalysis by **1**·[Rh(NBD)]X and **1**·[Rh(ETH)$_2$]X (X = Cl and $BF_4$) was studied in the gas phase (2 bar, 46°C) to reveal that **1**·[Rh(ETH)$_2$]($BF_4$) was the most active catalyst (TOF = 64 hr$^{-1}$); the NBD starting materials and the chloride salt were notably less active. Based on these observations, the activity of the Rh(I) bis(ethylene) complexes, **1**·[Rh(ETH)$_2$]$BF_4$ and **1**·[Rh(ETH)$_2$]Cl, in butene isomerization was also studied using gas-phase NMR spectroscopy. Under one bar of butene at 46°C, **1**·[Rh(ETH)$_2$]$BF_4$ rapidly catalyses the conversion of 1-butene to 2-butene with a TOF averaging 2000 hr$^{-1}$ over five cycles. Notably, the chloride derivative, **1** [Rh(ETH)$_2$]Cl displays negligible activity in comparison. XPS analysis of the post-catalysis sample, supported by DFT calculations, suggest that the catalytic activity is inhibited by the strong interactions between a Rh(III) allyl hydride intermediate and the chloride anion.

## Introduction

Metal-organic Frameworks (MOFs) are a class of network solids comprised of metal nodes interconnected by chemically and structurally mutable organic links.[1-3] A salient feature of MOF chemistry is that their robust porosity, stability and chemical functionality can be controlled via the considered selection of the organic and inorganic building blocks.[3] These design principles, termed 'reticular chemistry', have led to the synthesis of materials tailored towards applications including gas separation,[4-7] sensing,[8-9] biotechnology[10-12] and catalysis.[1-3, 13-17] With respect to catalysis, MOF synthesis offers a straight-forward approach to incorporating homogeneous systems within a heterogeneous environment.[12, 18] This can be achieved via incorporating pre-synthesized homogeneous species into the MOF network or post-synthesis metalation of suitably functionalized organic links. A recent, representative, example of the former is the heterogenization of the molecular iridium complex, [Ir(bipy)$Cl_3$(THF)], for $CO_2$ hydrogenation.[19] The same research group have also shown that post-synthesis metalation can be successfully applied to stabilize coordinatively unsaturated Ir species for methane activation.[20] In general, these strategies have been widely employed for the synthesis of MOF catalysts or for exploring chemical reactions within their pore networks.[21-25]

Incorporating molecular catalysts into a porous MOF architecture facilitates the exploration of their gas phase reactivity. However, although MOF chemistry offers unprecedented opportunities for transposing homogeneous organometallic catalysts to a porous heterogeneous environment, examples of single-site, gas

phase, organometallic chemistry in MOFs are rare.[26] This observation is intriguing as related work on solid-state organometallic complexes has shown that a solvent free environment allows for highly reactive species to be examined.[27-33] For example, Weller and co-workers have applied this strategy to elucidate the structure of an elusive transition-metal σ–alkane complex and develop solid-state catalysts that operate in the gas phase.[30, 34] Though experiments performed on well-defined, single molecules in the solid-state have provided insight into bond activation and catalytic processes, MOFs offer a clear advantage for exploring solid/gas chemistry. Namely, their 'node' and 'linker' modular synthesis gives rise to, robust, porous networks of predetermined structure metrics. Thus, a reactive metal complexes can be site-isolated within a porous network of predetermined porosity. In contrast, the arrangement of molecules in a crystal are determined by supramolecular crystal packing forces and are yet to be controlled or predicted with precision. Moreover, the structures are typically sensitive to solvent removal under reduced pressure or temperature, i.e. they lack permanent porosity.

We have recently shown that a Manganese-based MOF, **1** ($[Mn_3(L)_2L']$, where L = bis(4-carboxyphenyl-3,5-dimethyl-pyrazol-1-yl)methane), is a promising system for examining chemical reactions confined within pore networks.[35-39] A key feature of **1** is the modulated flexibility of the organic linker[40] which can accommodate structural perturbations associated with post-synthesis metalation and subsequent chemical reactions at the metal site with retention of crystallinity. [35-39] As a result, single crystal X-ray diffraction (SCXRD) can be employed to precisely study chemistry within the MOF. Importantly, such atomic level insight is crucial to develop our knowledge of how nanoporous environments can modify chemical reactivity. To this end we sought to incorporate well-defined Rh(I) olefin species into **1** due to their potential to carry out solid/gas reactions of commercial interest. Organometallic Rh(I) complexes bearing olefin ligands have been previously isolated on solid supports including alumina,[41] zeolites[42-46] and MOFs.[47] However, their precise structural characterization by SCXRD was not possible because these species lacked long range order. Here we report the synthesis, characterization and reactivity of a series of $[Rh(olefin)]^+$ species bound to the pyrazole groups of **1**. We show that **1**·$[Rh(ETH)_2](BF_4)$ is a highly active (average $TOF^{90\%}$ ca. 2000 $h^{-1}$ over five cycles) and recyclable catalyst for the low temperature gas phase isomerization of 1-butene to 2-butene, a reaction of interest in alkane upgrading processes; notably however, the Cl salt is essentially inactive. This work exemplifies how a well-defined organometallic complex can be incorporated and stabilized within a MOF and carry out efficient, cycled catalysis in the gas phase. The exceptional catalytic performance of this system highlights that MOFs are an excellent platform material for the design of bone fide single atom catalysis in the solid-state.

## Results and Discussion

Post-synthetic metalation (PSM) is known to be an effective strategy for incorporating metal complexes into the pore networks of MOFs.[18, 48-49] We have previously reported that the *N*,*N*-chelation site of as-synthesized **1** is metal free and thus poised for PSM via the open channels of the structure.[35, 37-40, 50] A remarkable feature of **1** is that PSM can be employed to bind transition metal complexes in solution with retention of crystallinity. Indeed, **1** can retain crystallinity after consecutive reactions at the tethered metal site, thus enabling structural elucidation of metalation products via SCXRD.[37, 39]

MOFs are known to be thermally stable over 773 K;[51-56] however, exposure to such conditions often results in structure degradation and loss of porosity. Furthermore, a number of common solvents are known to play a role framework decomposition,[57] and structural transformations.[58-59] Thus, we sought to design a MOF-based catalyst for application in reactions that operate in the gas phase at temperatures mild enough to allow for the intrinsic properties of the network to be retained, i.e. porosity and crystallinity. Light hydrocarbon processing is of significant commercial interest and there a number of organometallic moieties that carry out alkene hydrogenation and isomerization under mild conditions.[60-62] These include a number of molecular Rh(I) species,[30, 63] however crystallographically well-defined solid-state systems are uncommon. We hypothesized that MOFs are excellent platform materials for transposing such homogeneous organometallic chemistry into the solid-state. By applying the well-established principles of reticular chemistry and PSM, single-site, organometallic catalysts poised to carry-out industrially favoured solid/gas hydrocarbon processing could be realized. Accordingly, we synthesized several forms of MOF **1** furnished with organometallic Rh(I) olefin complexes and examined their catalytic reactivity towards the hydrogenation and isomerization of alkenes.

Reaction between **1** and $[Rh(ETH)_2Cl]_2$ or $[Rh(NBD)Cl]_2$ yields the corresponding cationic complexes **1**·$[Rh(NBD)][Rh(NBD)Cl_2]$ (**1**·NBD, NBD = norbornadiene) and **1**·$[Rh(ETH)_2][Rh(ETH)_2Cl_2]$ (**1**·ETH) quantitatively as pale yellow crystals. Due to the sensitivity of $[Rh(ETH)_2Cl_2]$ towards ligand displacement and subsequent decomposition in solution, we conducted the reaction between **1** and the Rh(I) precursor at 40˚C in ethanol (EtOH) under an atmosphere of ethylene in a sealed glass pressure tube (Figure 1). These conditions afforded **1**·$[Rh(ETH)_2][Rh(ETH)_2Cl_2]$ as yellow crystals. It is worth noting that reaction in acetonitrile (MeCN) resulted in loss of the ethylene ligands and formation of the corresponding bis-acetonitrile complex, **1**·$[Rh(MeCN)_2]Cl$ (structurally characterized following anion exchange with NaCl in MeCN) (SI Figure 5.3.7).

In each case, quantitative metalation was determined by Energy Dispersive X-ray (EDX) analysis, which revealed the expected 3:2 Mn:Rh ratio (SI. 1.0). Subsequent to PSM the MOF crystals retain their crystallinity, allowing the coordination sphere of the Rh(I) complexes to be elucidated using SCXRD; additionally, bulk sample crystallinity was confirmed by powder X-ray diffraction (PXRD) analysis, see SI Figure 4.1 and 4.4. The structure data of **1**·$[Rh(NBD)][Rh(NBD)Cl_2]$ revealed the expected square planar coordination geometry for a $d^8$ Rh(I) moiety. Specifically, the NBD ligand chelates the Rh centre, both of

which lie on a mirror plane, with Rh–C bond lengths of 2.167(13)/2.094(8) Å that are comparable to those observed in analogous molecular materials.[64-66] The

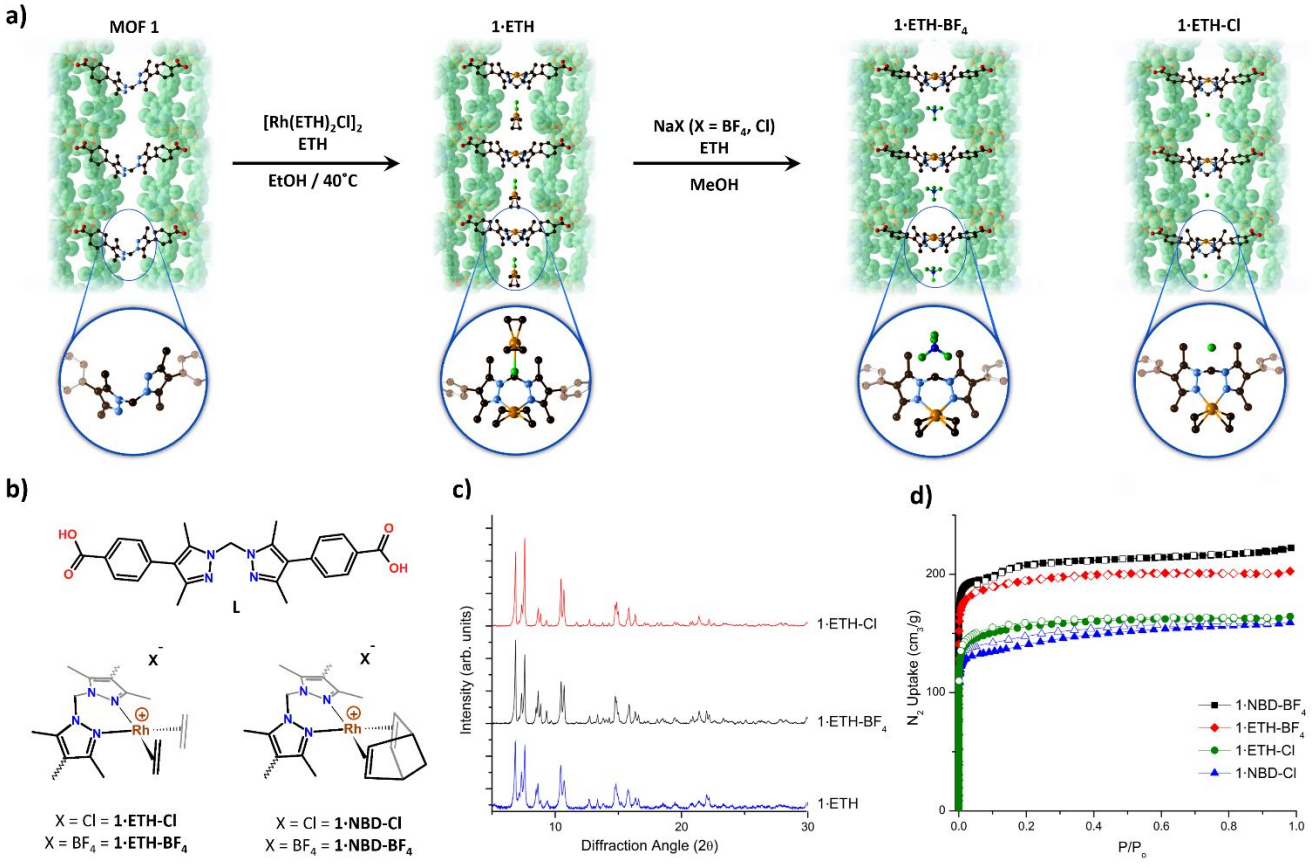


**Figure 1. a)** The metalation of **1** with $[Rh(ETH)_2Cl]_2$ proceeds to form the corresponding **1**·$[Rh(ETH)_2][Rh(ETH)_2Cl_2]$ complex and anion exchange with $NaBF_4$ or NaCl yields the corresponding $BF_4$ or Cl complexes respectively. The charge balancing anions ($[Rh(ETH)_2Cl_2]$, $BF_4$, Cl) all occupy the same position in the MOF pore adjacent the coordinated Rh centre stabilized by a series of weak C-H·anion hydrogen bonds with the MOF. For clarity, the MOF is presented as a green van der Waals surface while the bridging ligand and chelated metal complex are presented in a ball and stick format (C, black; N, pale blue; Cl, green; Rh, orange; B, blue; F, green). **b)** Representations of the MOF ligand (L) and the chelated Rh sites described herein. **c)** PXRD plots of **1**·ETH, **1**·ETH-Cl and **1**·ETH-$BF_4$ indicating retention of crystallinity and **d)** $N_2$ isotherms collected at 77K for each Rh(I) metalated sample.

complexes are charge balanced by a $[Rh(NBD)Cl_2]^-$ anion which occupies a pocket in the MOF pore adjacent to the *N,N*-chelated Rh(I) cation. In the case of **1**·$[Rh(ETH)_2][Rh(ETH)_2Cl_2]$, refinement of the structural model confirmed the presence of the *N,N*-chelated $[Rh(ETH)_2]^+$ cation and an accompanying $[Rh(ETH)_2Cl_2]^-$ anion. The Rh-C bond lengths are 2.13(2) and 2.05(3) Å, which again is in agreement with equivalent interactions in other Rh(I) ethylene complexes.[67-68] It is worth mentioning that this is a rare example of a Rh(I) bis-ethylene complex supported by an N-donor ligand system,[67-68] highlighting that the MOF can act as a matrix for the isolation of kinetically unstable transition metal complexes.[39, 69] We also note that the $[Rh(ETH)_2Cl_2]$ anion is uncommon and has only been reported recently (Rh-C bond lengths of 1.985(18) and 2.215(16) Å).[70]

Prior to examining the catalytic performance of metalated forms of **1** it is essential that the $[Rh(olefin)Cl_2]$ anions are removed as they provide extraneous reactive sites. Facile and quantitative anion exchange of $[Rh(olefin)Cl_2]$ with $NaBF_4$ or NaCl was achieved by soaking single crystals of **1**·$[Rh(NBD)][Rh(NBD)Cl_2]$ or **1**·$[Rh(ETH)_2][Rh(ETH)_2Cl_2]$ in methanol solutions of $NaBF_4$ or NaCl (Figure 1a for the ethylene complexes). However, for the more sensitive bis(ethylene) species, **1**·$[Rh(ETH)_2][Rh(ETH)_2Cl_2]$, the anion exchange process was performed under an ethylene atmosphere to prevent decomposition of the complex. Samples of the four Rh(I) functionalized species, **1**·$[Rh(NBD)](BF_4)$ (**1**·NBD-$BF_4$), **1**·[Rh(NBD)]Cl (**1**·NBD-Cl), **1**·$[Rh(ETH)_2](BF_4)$ (**1**·ETH-$BF_4$) and **1**·$[Rh(ETH)_2]$Cl (**1**·ETH-Cl), were examined via EDX analysis (SI 1.0) to confirm quantitative exchange of the $[Rh(olefin)Cl_2]$ anion for Cl or $BF_4$. Following the two-step PSM and anion exchange process the MOF crystals retain their crystallinity, as confirmed via PXRD analysis (Figure 1 and SI Figures 4.1 and 4.4). We then employed SCXRD to elucidate the coordination environment of the resulting Rh(I) species. **1**·NBD-$BF_4$ and **1**·NBD-Cl were solved in the monoclinic space group $P2_1/c$, with the diene ligand retaining a canted binding motif with Rh-C bond lengths for the alkene groups

of 2.111(4)/2.135(4) and 2.141(4)/2.124(5) Å, and 2.159(12)/2.110(15) and 2.189(12)/2.100(10) Å for the $BF_4$ and Cl salts respectively (Figure 2a, these structures lack the mirror symmetry of the precursor which contains the [Rh(NBD)$Cl_2$] anion). The canting of the NBD ligands avoids steric encumbrance from the methyl groups of the MOF linker. For both **1**·NBD-$BF_4$ and **1**·NBD-Cl, the $BF_4$ and Cl anions, respectively, reside in a pocket within the MOF pore previously occupied by the [Rh(L)$Cl_2$]$^-$. We note that this pocket is commonly occupied by anions[36-37] due to the presence of multiple weak C-H·anion interactions. The anion exchanged samples **1**·ETH-$BF_4$ and **1**·ETH-Cl crystallized in the monoclinic space group $P2_1/m$. Rh-ethylene bond lengths refined to 2.26(3)/2.10(3) Å and 2.18(2)/2.072(10) Å, respectively for the Cl and $BF_4$ salts, and the Cl and $BF_4$ anions are located within the same pocket as the NBD analogues. To the best of our knowledge, the only other examples in which a M(ethylene)$_2$ (M = Rh, Ir) moiety has been incorporated within a MOF feature dispersed complexes bound to the nodes of Zr(IV) based frameworks and these sites were not able to be characterized by SCXRD.[43, 71-72]

The bulk crystallinity and permanent porosity of the Rh(I) olefin species were assessed by performing PXRD measurements and gas adsorption isotherms, respectively. Samples of **1**·NBD-$BF_4$ and **1**·NBD-Cl were solvent exchanged with acetone and then heated at 80°C for 20 hr. PXRD analysis of samples following removal of pore solvent confirmed that crystallinity was retained (SI Figure 4.5-4.6). 77K $N_2$ gas adsorption isotherms were performed on **1**·NBD-$BF_4$ and **1**·NBD-Cl (Figure 1) and BET analysis was applied to the data. Surface areas of 808 and 539 $m^2/g$ were obtained for **1**·NBD-$BF_4$ and **1**·NBD-Cl respectively, albeit lower than expected for the Cl salt. These values are; however, in broad agreement with surface areas observed for other metalated derivatives of **1**.[35] Crystalline samples of **1**·ETH-$BF_4$ and **1**·ETH-Cl were washed with pentane and placed under vacuum for 2 hrs. 77K $N_2$ isotherms were collected and BET analysis of the data yielded surface areas of 732 and 562 $m^2/g$ for **1**·ETH-$BF_4$ and **1**·ETH-Cl respectively (Figure 1). The composition of the samples used for these adsorption analyses was examined via gas phase NMR spectroscopy. For samples of **1**·ETH-$BF_4$ and **1**·ETH-Cl exposure to CO/Me (1:1, 2 bar) displaced the coordinated ethylene, which was measured by integration against the methane signal in the gas phase, and demonstrated retention of approximately two ethylene ligands within the coordination sphere of the Rh for both samples (SI 7.3). PXRD analysis also confirmed that both materials retain crystallinity (SI Figure 4.2-4.3).

. The similar differential between the surface areas of the $BF_4$ and Cl samples for both sets of Rh(I)-metalated MOFs prompted us to further consider the structures. Geometric surface areas were calculated for all species (taking into account the various disorder models, (see Table S9) and in both cases the Cl salt has a lower surface area than the $BF_4$ sample; approximately 15% lower for the NBD and 7% lower for the bis(ethylene) forms. Calculated pore volumes reflect these trends also (Table S9).

**Gas phase alkene hydrogenation**

We examined the reaction between activated samples of **1**·ETH-$BF_4$, **1**·ETH-Cl, **1**·NBD-Cl and **1**·NBD-$BF_4$ and $H_2$ in the gas phase. The yellow crystals of **1**·ETH-$BF_4$ and **1**·ETH-Cl turn black instantaneously whilst **1**·NBD-$BF_4$ and **1**·NBD-Cl become black after 1 and 6 hrs, respectively. Despite this, the MOF crystals remained in excellent condition, allowing SCXRD data to establish that Rh was no longer coordinated to the *N,N*-chelating site of the MOF. Transmission Electron Microscopy (TEM) and Selected Angle Diffraction (SAD) analysis confirmed that in the presence of $H_2$ the Rh cations had undergone reduction to Rh(0) nanoparticles with an average diameter of 7 nm (**1**·NP) (See SI 2.0 and SI 3.0 for details). The 7 nm diameter of the Rh nanoparticles appears to be dictated by the pore size of the MOF structure (*ca*. 1 nm pore diameter), as observed for other systems where only a low density of the metal source is provided.[73] Despite varying the reaction temperature, $H_2$ pressure or performing the hydrogenation reaction in solution, nanoparticle formation could not be averted. These data suggest that the *N,N*-chelated Rh(I) centre is unstable towards $H_2$ once the alkene is hydrogenated.

We hypothesized that the presence of excess alkene would prevent nanoparticle formation by stabilising the Rh(I) sites to $H_2$ reduction, thereby facilitating gas-phase alkene hydrogenation. Thus, we examined the catalytic hydrogenation of ethylene by **1**·NBD-$BF_4$, **1**·NBD-Cl, **1**·ETH-$BF_4$ and **1**·ETH-Cl under conditions of excess alkene (Figure 2). Reactions were conducted in gas-tight NMR tubes and the headspace of the tube was monitored via $^1$H NMR spectroscopy. Each sample (~2-3 mg of known mass) was exposed to a mixture of ethylene (1.2 bar, 140 μmol) and $H_2$ (0.8 bar, 95 μmol), giving a Rh loading of ~2 mol% based on $H_2$ content. **1**·ETH-$BF_4$ showed rapid ethylene hydrogenation at 46°C, consuming the available hydrogen within 25 minutes (Figure 2, $TOF^{90\%}$ of 64 $h^{-1}$). Under these conditions, the catalytic activity is limited by the excess of ethylene, and improved activity can be achieved by using a greater portion of $H_2$ in the reaction mixture; however, those conditions lead to nanoparticle formation (vide supra). Catalyst cycling was investigated by placing the NMR tube under vacuum for 3 minutes before dosing with fresh

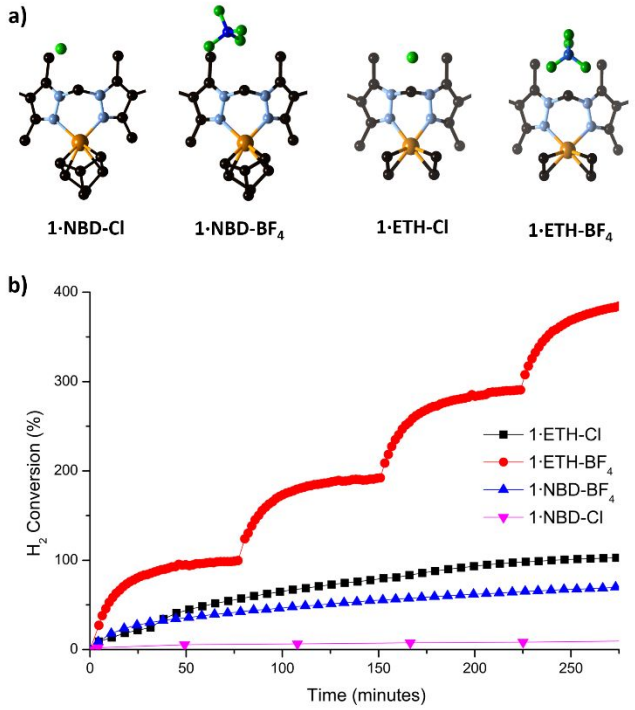


**Figure 2. a)** X-ray crystal structures of the Rh(I) site in **1**·NBD-Cl, **1**·NBD-$BF_4$,·**1**·ETH-Cl and **1**·ETH-$BF_4$. **b)** Hydrogenation of ethylene catalyzed by the family of **1**·[Rh(olefin)$_2$] complexes. **1**·ETH-$BF_4$ is the most active catalyst (plot truncated), while the NBD compounds show much lower activity.

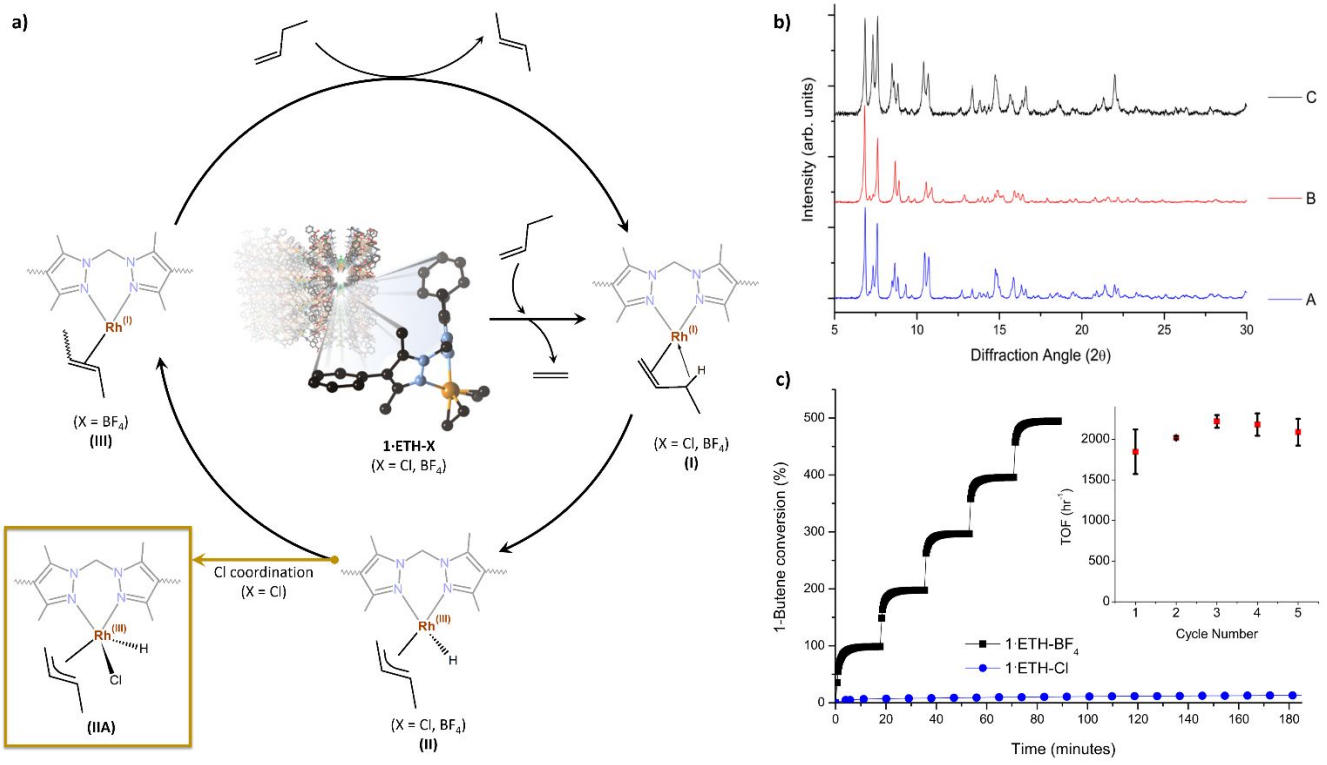


**Figure 3. a)** The proposed mechanism for 1-butene isomerization catalyzed by **1**·ETH-$BF_4$ with (inset) the proposed inactive Rh(III) intermediate formed upon reaction of **1**·ETH-Cl with 1-butene. **b)** PXRD data for **1**·ETH-$BF_4$ initial (A), activated (B) and after butene isomerization catalysis (C). **c)** Butene isomerization catalyzed by **1**·ETH-$BF_4$ over five successive cycles (black curve), whereas the analogous chloride complex **1**·ETH-Cl displays negligible activity in comparison (blue curve). The inset shows butene isomerization $TOF^{95\%}$ for **1**·ETH-$BF_4$ over five consecutive cycles.

$H_2$/ethylene. **1**·ETH-$BF_4$ maintained activity over 5 cycles (TOF 44 $h^{-1}$ on the fifth cycle), the crystals remained yellow, and PXRD analysis confirmed that the MOF had retained crystallinity and overall structure during the catalytic cycles.

Intriguingly, the chloride derivative, **1**·ETH-Cl displayed markedly lower activity (Figure 2) than its $BF_4$-counterpart,

suggesting that the stronger coordinating anion significantly impacts the activity of the Rh centre. Indeed, XPS analysis of **1**·ETH-Cl post hydrogenation shows that chlorine anions (Cl 2p peak maximum centred at 199 eV ) are likely bonded to the Rh site (See SI 10.0, Figure 10.1). Furthermore, the IR spectrum of the catalyst post hydrogenation possesses weak bands centred at 2026 and 1934 $cm^{-1}$ that may be attributed to a Rh(III)-hydride moiety (SI Figure 8.2).[74-75] Collectively, these data support the presence of a chloride in the coordination sphere of a Rh(III) species that deactivates the catalyst, whereas the weakly coordinating $BF_4$ does not bind to the Rh and thus facilitates catalysis.

The diene samples, **1**·NBD-$BF_4$ and **1**·NBD-Cl displayed significantly lower activity for ethylene hydrogenation than **1**·ETH-X, failing to reach complete conversion of $H_2$ after 9 hrs. This can be attributed to the slow kinetics of NBD hydrogenation required to generate the active Rh(I) catalyst.[76] Additionally, hydrogenation of the NBD samples follows the same anion dependency as their ethylene counterparts: the chloride anion significantly reduces the catalytic activity of the Rh(I) complex. Similar behaviour has been reported for homogeneous olefin hydrogenation using Ir(I) catalysts, which display negligible activity in the presence of halide anions.[77]

Finally, we investigated the activity of activated **1**·NP towards ethylene hydrogenation. In line with its retention of porosity (SI Figure 6.1), **1**·NP displayed good ethylene hydrogenation activity in the first cycle ($TOF^{90\%}$ = 32 $h^{-1}$), but this activity was considerably diminished in the second cycle ($TOF^{90\%}$= 9 $h^{-1}$) highlighting the importance of retaining the active single atom Rh(I) centre. (SI Figure 7.1.1)

**Gas phase alkene isomerization**

Rh(I) ethylene complexes are known to catalyse the isomerization of 1-butene to 2-butene, which is a valuable precursor in the synthesis of 2,3-butanediol used as a cross-linking agent in rubber manufacturing.[78] Single crystals of organometallic Rh(I) species are known to successfully isomerize 1-butene in the solid-state (room temperature, 1 bar). However, the porosity of these structures is serendipitous and realized via weak, intrinsically fragile, crystal packing forces. We postulated that the permanent porosity of **1**·ETH would provide an ideal platform for gas-phase butene isomerization (SI 11.1), owing to the accessibility of the Rh centres and permanent porosity of **1**. Moreover, we anticipated that **1**·ETH-$BF_4$ and **1**·ETH-Cl would display disparate activity based on the presence of non- or weakly coordinating $BF_4$ and coordinating $Cl^-$ anions respectively, as observed under hydrogenation conditions.

Samples of **1**·ETH-$BF_4$ and **1**·ETH-Cl were activated in NMR tubes using the same protocol described above. 1-Butene (1 bar, 86 μmol) was subsequently added to the tube, which was sealed, and the conversion of 1-butene to 2-butene was monitored via gas-phase NMR spectroscopy (46˚C). **1**·ETH-$BF_4$ rapidly catalyses the conversion, reaching the thermodynamic limit (98%) within 9 minutes with a $TOF^{90\%}$ of ca. 1845 ±275 $h^{-1}$ (Figure 3). Over the course of five successive cycles, the activity is retained (average $TOF^{90\%}$ of ca. 2000 $h^{-1}$), demonstrating that the host framework is capable of maintaining site-isolation and activity of the Rh centres.

As predicted, the chloride analogue **1**·ETH-Cl displays negligible activity in butene isomerization at 46˚C; reaching 5% conversion in the initial minutes of the reaction but achieving only 19% conversion over the ensuing 9 hours (Figure 3). As the sample remains porous (SI Figure 6.2), such rapid inactivation points to the involvement of the chloride anion in the formation of a catalytically incompetent species during the initial stages of catalysis (within the first ~2 cycles considering the initial 5% conversion). The mechanism of butene isomerization is proposed to proceed via a C-H activation of the $CH_2$ functionality adjacent to the alkene, forming an Rh(III) allyl hydride which undergoes reductive elimination to yield 2-butene (Figure 3).[30] We hypothesized that the formation of a Rh(III) allyl hydride intermediate would provide an opportunity for the adjacent chloride anion to bind, generating a stable Rh(III) complex and thereby inhibiting catalytic activity.

To examine anion interference, DFT calculations were employed to explore the energy landscape of the proposed butene isomerization mechanism, using a representative molecular analogue of the MOF bound Rh site (SI 11.0). Starting at the 1-butene bound cation I (4.95 kJ $mol^{-1}$), oxidative cleavage of the C–H bond proceeds with a barrier of 36.6 kJ $mol^{-1}$ to give allyl-cation II (12.2 kJ $mol^{-1}$). The subsequent C-H activation has a barrier of 14.7 kJ $mol^{-1}$ to produce the 2-butene bound cation III (0.00 kJ $mol^{-1}$). This modest overall barrier of 36.6 kJ $mol^{-1}$ is consistent with analogous chemistry.[30] The key steps (giving species II and III) for this reaction were further investigated in the presence of $BF_4$ and Cl counter anions. These simulations confirm that chloride (Figure 3, inset) significantly stabilizes the Rh(III) allyl complex by more than 80 kJ $mol^{-1}$ (relative to the butene bound complexes). In contrast the $BF_4$ anion only stabilizes the Rh site by approximately 30 kJ $mol^{-1}$, relative to the two butene complexes. These data support the experimental results that show the chloride complex is catalytically incompetent. Further, we performed XPS and IR analysis on **1**·ETH-Cl after exposure to 1-butene to experimentally probe the putative chloride bound species. The XPS data provides evidence of Cl anions bound to the Rh site in a 1:1 ratio (SI Figure 10.1) whilst the IR shows the presence of two weak bands at 2000 and 2036 $cm^{-1}$ that can be attributed to ν(Rh-H stretch) of the **1**·[Rh($C_4H_7$))(H)(Cl)] species (SI Figure 8.1).[74-75] In contrast, no such stretch was observed in the case of the $BF_4$ analogue. In summary, DFT, XPS and IR spectroscopy collectively support that chloride coordination to the Rh(III) allyl hydride intermediate occurs in **1**·ETH-Cl and is responsible for the comparatively poor catalytic performance.

We sought to determine whether the catalysis occurs within the pore network or primarily at the surface of the MOF crystals. To this end we finely crushed single crystals of **1**·ETH-$BF_4$ were prepared by placing a sample of **1**·ETH-$BF_4$ (pentane solvated) in a glass pressure tube under an ethylene atmosphere and stirring rapidly with a magnetic stirrer to crush the crystals. If catalysis is primarily surface-based one would expect that activity would increase due to

increased surface area;[30] however, if catalysis occurred within the MOF pores (in addition to the surface) and mechanical stress led to partial collapse of the framework structure we would anticipate activity would diminish. Accordingly, we performed a butene isomerization experiment on a sample of finely crushed crystals. Catalytic activity was notably reduced by ca. one order of magnitude ($TOF^{90\%}$ 219 $hr^{-1}$). We then collected a 77K $N_2$ isotherm to ascertain if the pore structure had been compromised by crushing. Close inspection of the data showed a significantly reduced uptake of $N_2$, with a BET surface area of 247 $m^2g^{-1}$ (SI Figure 6.3, compared with 732 $m^2/g$ prior to crushing) confirmed that the pore access was restricted in this sample. These results suggest that the robust, open, porous structure of the MOF scaffold is integral to the gas phase catalytic activity of the material as it allows access of the substrate to all of the Rh active sites. To ascertain that all the **1**·ETH-$BF_4$ catalytic sites are accessible in a pristine sample we examined the diffusion of 1-butene within the MOF pore network using classical molecular dynamics simulations. Close inspection of the computational results showed that diffusion of 1-butene is unrestricted in **1**·ETH-$BF_4$, thus underscoring the importance of the open network for reactive site accessibility. The diffusion of the 2-butene product is somewhat restricted and would occur more slowly, possibly indicating that the diffusion of the product out of the MOF structure is a limiting factor in the gas phase catalytic activity.

## Conclusion

Here we showed that the intrinsic properties of MOF materials, high crystallinity and robust porosity, coupled with reticular synthesis principles facilitate the design of solid-state single-site organometallic catalysts for commercially relevant gas phase reactions. Indeed, **1**·ETH-$BF_4$ is a highly efficient catalyst for the isomerization of 1-butene (average $TOF^{90\%}$ ca. 2000 $hr^{-1}$). Additionally, due to the rigid MOF architecture, the catalyst can be cycled without a measurable loss of activity. Although some homogeneous catalysts show higher TOFs,[79-81] up to (8600 $hr^{-1}$), they are prone to decomposition.[79] While known examples of nanoparticle-based heterogeneous catalysts show comparable activity, these operate at higher temperatures. Thus, due to the MOF scaffold, gas phase catalysis by reactive organometallic entities can be conducted under mild conditions without decomposition. Furthermore, the reticular design principles inherent to MOF chemistry can allow for outer-sphere interactions to be tailored[82] which could have a marked influence on the chemo-, stereo-, and regioselectivity of chemical transformations.

## Experimental

### General Experimental Considerations

Single crystals of MOF **1** were prepared as previously reported.[35] The chemicals ethylene, 1-butene, $[Rh(NBD)_2Cl]_2$, $[Rh(ETH)_2Cl]_2$ were purchased from commercial vendors and used as received. Samples were handled under standard Schlenk techniques unless otherwise stated. Solvents were dried using literature procedures and degassed with Ar prior to use. Specifically, MeCN was dried from $CaH_2$ under nitrogen; EtOH and methanol (MeOH) were dried by refluxing them over Mg under $N_2$; acetone was dried from $CaSO_4$ under nitrogen; and pentane was dried over Na/benzophenone. $NaBF_4$ and NaCl used for anion exchange were stored in a 120˚C drying oven.

Powder X-ray diffraction (PXRD) data were collected on a Bruker Advanced D8 diffractometer (capillary stage) using Cu Kα radiation (λ = 1.5456 Å , 40 kW/ 40mA, 2θ = 2 – 52.94°, phi rotation = 20 rotation/min, at 1 sec exposure per step with 5001 steps and using 0.5 mm glass capillaries). Solution NMR spectra were recorded on Varian 500 or 600 MHz instruments at 23°C using a 5 mm probe. Gas phase NMR spectra were collected on a Varian Gemini 600MHz NMR spectrometer as described below. Infrared (IR) spectra were collected on a Perkin-Elmer Spectrum Two, with the sample distributed between two NaCl disks in Nujol. High-resolution transmission electron microscopy (HRTEM) images and diffraction pattern were acquired using an uncorrected FEI Titan Themis 80-200. Energy dispersive X-ray spectroscopy (EDX) was performed on a Philips XL30 field emission scanning electron microscope. Gas adsorption isotherm measurements were performed on an ASAP 2020 Surface Area and Pore Size Analyser. Activation of samples was carried out as described.

### Preparation of 1·[Rh(NBD)][Rh(NBD)$Cl_2$] (1·NBD)

Single crystals of **1** (~24 mg) were placed in a 4 ml glass vial and washed with freshly distilled acetonitrile under Ar flow a total of 5 times (the solution was degassed with Ar after each exchange and the sample was allowed to soak for 1hr between washings). Under Ar flow, $[Rh(NBD)Cl]_2$ (30 mg) was added and the vial was sealed under Ar and heated at 65°C for 16 hrs. The resulting yellow crystals were washed with freshly distilled acetonitrile five times under Ar flow to give **1**·NBD as yellow crystals. IR $\nu_{max}$ (nujol, $cm^{-1}$): 1612 (s, C=C), 1556 (m, C=C), 1458 (m, C=C) 1408, 1376.

### Anion Exchange Protocols for 1·NBD-$BF_4$ and 1·NBD-Cl

Single crystals of **1**·NBD (~24 mg) were placed in a 4 ml glass vial and washed with freshly distilled methanol under Ar flow a total of 5 times (the solution was degassed with Ar after each exchange and the sample was allowed to soak for 1 hr between washings). Dry $NaBF_4$ or NaCl (~300 mg) was added to a small glass ampule which was subsequently submerged in the 4 ml vial containing the MOF sample. The solution was degassed with Ar, the vial was sealed and allowed to stand at room temperature (RT) for 48 hrs ($BF_4$) and 7 days (Cl). Under Ar flow, the ampule containing undissolved salt was removed and the yellow MOF crystals were washed with freshly distilled methanol five times under Ar flow.

**1**·NBD-$BF_4$: IR $\nu_{max}$ (nujol, $cm^{-1}$): 1614 (s, C=C), 1556 (m, C=C), 1452 (m, C=C) 1405, 1376.

**1**·NBD-Cl: IR $\nu_{max}$ (nujol, $cm^{-1}$): 1611 (s, C=C), 1556 (m, C=C), 1457 (m, C=C) 1409, 1377.

### Preparation of 1·[Rh($CH_2CH_2$)$_2$][Rh($CH_2CH_2$)$_2Cl_2$] (1·ETH)

Single crystals of **1** (~24 mg) were placed in a 20ml glass pressure vessel fitted with a pressure gauge and Swagelok tap assembly (See SI 9.0 for details). The crystals were

washed with freshly distilled ethanol (5 x 5 ml) under Ar flow a total of 5 times (the solution was degassed with Ar after each exchange and the sample was allowed to soak for 1hr between washings). The solution was degassed with ethylene, excess $[Rh(ETH)_2Cl]_2$ (30 mg) was added and the pressure tube was sealed under ethylene (~1.2 bar) and heated at 40˚C for 24 hr. The resulting yellow crystals were washed with freshly distilled, ethylene degassed ethanol (5 x 5 ml) to remove dissolved Rh precursor. Insoluble Rh by-products were removed by washing the MOF crystals with dry, ethylene degassed acetone (5 x 5 ml) under ethylene flow to give **1**·ETH as yellow crystals. IR $\nu_{max}$ (nujol, $cm^{-1}$): 1610 (s, C=C), 1555 (m, C=C), 1458 (m, C=C) 1376, 1306.

### Anion Exchange Protocols for 1·ETH-$BF_4$ and 1·ETH-Cl

Single crystals of **1**·ETH (~24 mg) were placed in a 20 ml glass pressure vessel fitted with a pressure gauge and tap assembly (see SI.9.0 for details) and washed with freshly distilled, ethanol degassed methanol (5 ml) under ethylene flow a total of 5 times (the solution was degassed with ethylene after each exchange and the sample was allowed to soak for 1hr between washings). Excess oven dried $NaBF_4$ or NaCl was added to a small glass ampule which was subsequently submerged in the glass pressure tube containing the MOF sample. The solution was degassed with ethylene, the pressure tube was sealed and allowed to stand at RT for 24 hrs ($BF_4$) or 6 days (Cl). Under ethylene flow, the ampule containing undissolved salt was removed and the yellow MOF crystals were washed with freshly distilled, ethylene degassed methanol (5 ml) five times under ethylene flow.

**1**·ETH-$BF_4$: IR $\nu_{max}$ (nujol, $cm^{-1}$): 1611 (s, C=C), 1553 (m, C=C), 1455 (m, C=C) 1374, 1305.

**1**·ETH-Cl: IR $\nu_{max}$ (nujol, $cm^{-1}$): 1612 (s, C=C), 1554 (m, C=C), 1457 (m, C=C) 1377, 1307.

### Preparation of 1·$[Rh(MeCN)_2]Cl$

Single crystals of **1** (~24mg) were placed in an 8 ml glass vial. The crystals were washed with freshly distilled acetonitrile (5 x 5 ml) under Ar flow a total of 5 times (the solution was degassed with Ar after each exchange and the sample was allowed to soak for 1 hr between washings). Excess $[Rh(ETH)_2Cl]_2$ (30 mg) was added and the vial was sealed under an Ar atmosphere and allowed to stand at RT for 72 hrs. The resulting yellow crystals were washed with freshly distilled, argon degassed acetonitrile (5 x 5 ml) to remove dissolved Rh precursor. The resulting crystals were washed again with freshly distilled acetonitrile (5 x 5 ml) under argon. A small glass vessel containing dry NaCl was submerged in the acetonitrile such that the NaCl could dissolve and access the MOF crystals. After 7 days, the undissolved NaCl was removed and the MOF crystals were washed with freshly distilled acetonitrile under argon (5 x 5 ml) to give **1**·$[Rh(MeCN)_2]Cl$ as yellow crystals. An X-ray crystal structure was collected on a single crystal following solvent exchange with distilled THF. IR $\nu_{max}$ (nujol, $cm^{-1}$): 2315 (w, Rh-N≡$CCH_3$), 2293 (w, free $CH_3C$≡N), 2251 (w, free $CH_3C$≡N), 1612 (s, C=O), 1555 (m, C=C), 1458 (m, C=C) 1407, 1376.

### Gas Phase Hydrogenation

**1**·NBD-X or **1**·NP crystals (~2 mg) were washed with freshly distilled acetone (5 x 5ml) under argon degas, allowing the crystals to soak for 1 hr between exchanges. The sample was pipetted under argon flow into a pre-weighed NORELL high-pressure NMR tube fitted with a young tap. The excess of acetone was removed and the NMR tube placed under vacuum and heated in an oil bath at 85˚C for 20 hr. The NMR tube was cooled to room temperature under vacuum and dosed with ethylene (1.2 bar, 140 μmol) followed by hydrogen (0.8 bar, 95 μmol). The NMR tube was sealed and placed in a Varian Gemini 600MHz NMR spectrometer pre-heated to 46˚C.

**1**·ETH-$BF_4$ and **1**·ETH-Cl (~2 mg) were washed with recently distilled acetone (previously degassed with ethylene) five times under ethylene, allowing the crystals to soak for 1 hr between exchanges. Consequently, the crystals were washed with distilled pentane (previously degassed with ethylene) five times under ethylene, soaked for 1 hr between each exchange. The sample was pipetted into a pre-weighed NORELL high-pressure NMR tube fitted with a young tap under ethylene flow. The excess pentane was removed before the NMR tube was placed under vacuum for 2 hrs. The NMR tube then was dosed with ethylene (1.2 bar, 140 μmol) followed by hydrogen (0.8 bar, 95 μmol). The NMR tube was sealed and placed in a Varian Gemini 600MHz NMR spectrometer pre-heated to 46˚C.

### Data Collection and Processing Details

Gas phase chemical shifts are referenced relative to reported data.[34] Before the collection the NMR was locked with a benzene ($C_6D_6$) charged NMR tube at 46 ˚C, which was then replaced with the pre-loaded high-pressure NMR tube. A T1 delay 25 s was used. The extent of conversion was calculated by the comparison of the reduction/disappearance in the integral of the alkene $CH_2$ resonance of ethylene (5.31 ppm) and hydrogen (4.57 ppm), and the appearance of the two $CH_3$ alkyl resonance of ethane (0.88 ppm).

### Gas Phase Alkene Isomerization

Samples of Rh(I) bis(ethylene) metalated **1** (~2mg) were washed as previously stated for the gas phase hydrogenation experiments. The crystals were loaded into a high-pressure NMR tube fitted with a Teflon stopcock and activated for 2hr under vacuum at RT. Following activation, the NMR tube was dosed with ethylene (1 bar) for 5 minutes and subsequently evacuated for 3 minutes. 1-Butene was added (1 bar, 86 μmol) and placed in a Varian Gemini 600MHz NMR spectrometer pre-heated to 46˚C.

A crushed sample of **1**·ETH-$BF_4$ was prepared by transferring a sample of **1**·ETH-$BF_4$ (~30mg) in pentane to a glass high pressure tube (See SI 9.1 for tube details) charged with ethylene and a magnetic stir-bar. The vessel was placed above a magnetic stirrer for 30 minutes, thereby generating a crushed sample of **1**·ETH-$BF_4$ which was transferred to a high-pressure NMR tube for catalytic activity analysis as described above.

### Data Collection and Processing Details

Gas phase chemical shifts are referenced relative to reported data.[30] Before the collection the NMR was locked with a benzene ($C_6D_6$) charged NMR tube at 46 ˚C, which was then replaced with the pre-loaded high-pressure NMR

tube. A T1 delay of 0.01 s with 4 scans was used to collect data for **1**·ETH-$BF_4$ and while a T1 delay of 25 s with 4 scans was used for **1**·ETH-Cl. The extent of conversion was calculated by the comparison of the reduction in the integral of the alkyl $CH_2$ resonance of 1-butene at 6.0 ppm and the appearance of the two alkene CH resonances from 2-butene at 5.25 ppm.

### Molecular simulations

Surface area and probe-occupiable volume was simulated for a probe radius of 1.82 Å (equivalent to the size of $N_2$) using the Zeo++ program.[83-84] A cluster model was derived for a representative Rh complex, where the framework was cleaved at the pyrazole C4 position and capped with methyl functionality. Geometry optimizations of the butene and allyl containing complexes used the BP86 density functional[85-86] and employed by the ORCA software package.[87-88] Coulomb with the chain of spheres exchange algorithms (RIJCOSX)[89] were employed for the efficiency of calculations and the segmented all-electron def2-TZVP(-f) basis set and def2-TZVP/J auxiliary basis set for all atoms were used.[90-91] This also included the def2 effective core potentials for rhodium. Tight SCF convergence criteria and a fine DFT integration grid (Grid6) were implemented to obtain reliable accuracy and dispersion corrections (D3-BJ) was applied.[92]

Frequency calculations were performed analytically, and each intermediate was identified as a stationary point (minimum structure) as characterized by the absence of imaginary frequencies. This analysis further provided the necessary correction to the Gibbs free energy to give the free energy of each structure at 298 K. The energetic barriers between these characterized intermediates (I, II ,III), were approximated using climbing image nudged elastic band (CI-NEB) approach with 6 images.[93]

Molecular dynamics simulations were performed on a fixed structure of a $2 \times 1 \times 2$ supercell of **1**·[$Rh(ETH)_2$]($BF_4$) using the RASPA software package.[94] Butene molecules were treated using the TraPPE potential[95] and framework dispersion interactions were treated using universal force field parameters.[96] Dynamics were simulated with the NVT ensemble at 300 K for 20 molecules of butene employing 1 fs timestep and 1000 ps equilibration, the butene mean-squared displacement was recorded for a subsequent 5000 ps.

Representative input files for molecular simulations are available online in the data repository https://github.com/jackevansadl/supp-data.

### Supporting Information

The Supporting Information is available free of charge on the ACS Publications website.
UV-visible spectroscopic data, powder X-ray diffraction data and additional information on the single crystal structures (PDF).
Crystallographic information files (cif) have been deposited with the Cambridge Crystallographic Database (CCDC). Deposition numbers 2003247-2003253. Full details are found in SI 5.0 with key parameters in SI Tables 5.2-5.4.

### Acknowledgment

CJS and CJD gratefully acknowledge the Australian Research Council for funding (DP160103234 and DP190101402). XSZ acknowledge the ARC for funding (FL170100101). J. D. E. acknowledges the support of the Alexander von Humboldt foundation and HPC platforms provided by a Grand équipement national de calcul intensif (GENCI) grant (A0010807069) and the Center for Information Services and High Performance Computing (ZIH) at TU Dresden. This research was undertaken in part using the MX1 and MX2 beamlines at the Australian Synchrotron, part of ANSTO, and made use of the Australian Cancer Research Foundation (ACRF) detector. RAP gratefully acknowledges Adelaide Scholarship International. We acknowledge the contribution of Peter Apoefis in developing the high-pressure reaction vessels used in this work (SI. 9.0).

### References

(1) Kitagawa, S.; Kitaura, R.; Noro, S. Functional porous coordination polymers. *Angew. Chem., Int. Ed. Engl.* **2004,** *43*, 2334.

(2) Furukawa, H.; Cordova, K. E.; O'Keeffe, M.; Yaghi, O. M. The chemistry and applications of metal-organic frameworks. *Science* **2013,** *341*, 974.

(3) Yaghi, O. M.; O'Keeffe, M.; Ockwig, N. W.; Chae, H. K.; Eddaoudi, M.; Kim, J. Reticular synthesis and the design of new materials. *Nature* **2003,** *423*, 705.

(4) Dechnik, J.; Sumby, C. J.; Janiak, C. Enhancing Mixed-Matrix Membrane Performance with Metal–Organic Framework Additives. *Cryst. Growth Des.* **2017,** *17*, 4467.

(5) Dechnik, J.; Gascon, J.; Doonan, C. J.; Janiak, C.; Sumby, C. J. Mixed-Matrix Membranes. *Angew. Chem., Int. Ed. Engl.* **2017,** *56*, 9292.

(6) Seoane, B.; Coronas, J.; Gascon, I.; Benavides, M. E.; Karvan, O.; Caro, J.; Kapteijn, F.; Gascon, J. Metal-organic framework based mixed matrix membranes: a solution for highly efficient $CO_2$ capture? *Chem. Soc. Rev.* **2015,** *44*, 2421.

(7) Mason, J. A.; Veenstra, M.; Long, J. R. Evaluating metal-organic frameworks for natural gas storage. *Chem. Sci.* **2014,** *5*, 32.

(8) Zhang, Y.; Yuan, S.; Day, G.; Wang, X.; Yang, X.; Zhou, H.-C. Luminescent sensors based on metal-organic frameworks. *Coord. Chem. Rev.* **2018,** *354*, 28.

(9) Cui, Y.; Chen, B.; Qian, G. Lanthanide metal-organic frameworks for luminescent sensing and light-emitting applications. *Coord. Chem. Rev.* **2014,** *273*, 76.

(10) Rogge, S. M. J.; Bavykina, A.; Hajek, J.; Garcia, H.; Olivos-Suarez, A. I.; Sepulveda-Escribano, A.; Vimont, A.; Clet, G.; Bazin, P.; Kapteijn, F.; Daturi, M.; Ramos-Fernandez, E. V.; Llabres, I. X. F. X.; Van Speybroeck, V.; Gascon, J. Metal-organic and covalent organic frameworks as single-site catalysts. *Chem. Soc. Rev.* **2017,** *46*, 3134.

(11) Wang, C.; An, B.; Lin, W. Metal–Organic Frameworks in Solid–Gas Phase Catalysis. *ACS Catal.* **2018,** *9*, 130.

(12) Drake, T.; Ji, P.; Lin, W. Site Isolation in Metal–Organic Frameworks Enables Novel Transition Metal Catalysis. *Acc. Chem. Res.* **2018,** *51*, 2129.

(13) Huang, Y. B.; Liang, J.; Wang, X. S.; Cao, R. Multifunctional metal-organic framework catalysts: synergistic catalysis and tandem reactions. *Chem. Soc. Rev.* **2016,** *46*, 126.

(14) Dhakshinamoorthy, A.; Garcia, H. Cascade reactions catalyzed by metal organic frameworks. *ChemSusChem.* **2014,** *7*, 2392.

(15) Dhakshinamoorthy, A.; Asiri, A. M.; Garcia, H. Metal-Organic Framework (MOF) Compounds: Photocatalysts for Redox Reactions and Solar Fuel Production. *Angew. Chem., Int. Ed. Engl.* **2016,** *55*, 5414.

(16) Ferey, G. Hybrid porous solids: past, present, future. *Chem. Soc. Rev.* **2008,** *37*, 191.

(17) Inokuma, Y.; Yoshioka, S.; Ariyoshi, J.; Arai, T.; Hitora, Y.; Takada, K.; Matsunaga, S.; Rissanen, K.; Fujita, M. X-ray analysis on the nanogram to microgram scale using porous complexes. *Nature* **2013,** *495*, 461.

(18) Manna, K.; Zhang, T.; Lin, W. Postsynthetic metalation of bipyridyl-containing metal-organic frameworks for highly efficient catalytic organic transformations. *J. Am. Chem. Soc.* **2014,** *136*.

(19) An, B.; Zeng, L.; Jia, M.; Li, Z.; Lin, Z.; Song, Y.; Zhou, Y.; Cheng, J.; Wang, C.; Lin, W. Molecular Iridium Complexes in Metal–Organic Frameworks Catalyze $CO_2$ Hydrogenation via Concerted Proton and Hydride Transfer. *J. Am. Chem. Soc.* **2017,** *139*, 17747.

(20) Feng, X.; Song, Y.; Li, Z.; Kaufmann, M.; Pi, Y.; Chen, J. S.; Xu, Z.; Li, Z.; Wang, C.; Lin, W. Metal-Organic Framework Stabilizes a Low-Coordinate Iridium Complex for Catalytic Methane Borylation. *J. Am. Chem. Soc.* **2019,** *141*, 11196.

(21) Zhang, T.; Manna, K.; Lin, W. Metal-Organic Frameworks Stabilize Solution-Inaccessible Cobalt Catalysts for Highly Efficient Broad-Scope Organic Transformations. *J. Am. Chem. Soc.* **2016,** *138*, 3241.

(22) Sawano, T.; Lin, Z.; Boures, D.; An, B.; Wang, C.; Lin, W. Metal-Organic Frameworks Stabilize Mono(phosphine)-Metal Complexes for Broad-Scope Catalytic Reactions. *J. Am. Chem. Soc.* **2016,** *138*, 9783.

(23) Zhang, X.; Huang, Z.; Ferrandon, M.; Yang, D.; Robison, L.; Li, P.; Wang, T. C.; Delferro, M.; Farha, O. K. Catalytic chemoselective functionalization of methane in a metal–organic framework. *Nature Catalysis* **2018,** *1*, 356.

(24) Dunning, S. G.; Nandra, G.; Conn, A. D.; Chai, W.; Sikma, R. E.; Lee, J. S.; Kunal, P.; Reynolds, J. E., 3rd; Chang, J. S.; Steiner, A.; Henkelman, G.; Humphrey, S. M. A Metal-Organic Framework with Cooperative Phosphines That Permit Post-Synthetic Installation of Open Metal Sites. *Angew. Chem., Int. Ed. Engl.* **2018,** *57*, 9295.

(25) Manna, K.; Zhang, T.; Greene, F. X.; Lin, W. Bipyridine- and Phenanthroline-Based Metal–Organic Frameworks for Highly Efficient and Tandem Catalytic Organic Transformations via Directed C–H Activation. *J. Am. Chem. Soc.* **2015,** *137*, 2665.

(26) Beloqui Redondo, A.; Morel, F. L.; Ranocchiari, M.; van Bokhoven, J. A. Functionalized Ruthenium–Phosphine Metal–Organic Framework for Continuous Vapor-Phase Dehydrogenation of Formic Acid. *ACS Catalysis* **2015,** *5*, 7099.

(27) Boyd, T. M.; Tegner, B. E.; Tizzard, G. J.; Martinez-Martinez, A. J.; Neale, S. E.; Hayward, M. A.; Coles, S. J.; Macgregor, S. A.; Weller, A. S. A Structurally Characterized Cobalt(I) sigma-Alkane Complex. *Angew. Chem., Int. Ed. Engl.* **2020,** *59*, 6177.

(28) McKay, A. I.; Martínez-Martínez, A. J.; Griffiths, H. J.; Rees, N. H.; Waters, J. B.; Weller, A. S.; Krämer, T.; Macgregor, S. A. Controlling Structure and Reactivity in Cationic Solid-State Molecular Organometallic Systems Using Anion Templating. *Organometallics* **2018,** *37*, 3524.

(29) Martínez-Martínez, A. J.; Tegner, B. E.; McKay, A. I.; Bukvic, A. J.; Rees, N. H.; Tizzard, G. J.; Coles, S. J.; Warren, M. R.; Macgregor, S. A.; Weller, A. S. Modulation of σ-Alkane Interactions in [Rh($L_2$)(alkane)]+ Solid-State Molecular Organometallic (SMOM) Systems by Variation of the Chelating Phosphine and Alkane: Access to $\eta^2$,$\eta^2$-σ-Alkane Rh(I), $\eta^1$-σ-Alkane Rh(III) Complexes, and Alkane Encapsulation. *J. Am. Chem. Soc.* **2018,** *140*, 14958.

(30) Chadwick, F. M.; McKay, A. I.; Martinez-Martinez, A. J.; Rees, N. H.; Kramer, T.; Macgregor, S. A.; Weller, A. S. Solid-state molecular organometallic chemistry. Single-crystal to single-crystal reactivity and catalysis with light hydrocarbon substrates. *Chem. Sci.* **2017,** *8*, 6014.

(31) Chadwick, F. M.; Kramer, T.; Gutmann, T.; Rees, N. H.; Thompson, A. L.; Edwards, A. J.; Buntkowsky, G.; Macgregor, S. A.; Weller, A. S. Selective C-H Activation at a Molecular Rhodium Sigma-Alkane Complex by Solid/Gas Single-Crystal to Single-Crystal H/D Exchange. *J. Am. Chem. Soc.* **2016,** *138*, 13369.

(32) Chadwick, F. M.; Rees, N. H.; Weller, A. S.; Kramer, T.; Iannuzzi, M.; Macgregor, S. A. A Rhodium-Pentane Sigma-Alkane Complex: Characterization in the Solid State by Experimental and Computational Techniques. *Angew. Chem., Int. Ed. Engl.* **2016,** *55*, 3677.

(33) Pike, S. D.; Thompson, A. L.; Algarra, A. G.; Apperley, D. C.; Macgregor, S. A.; Weller, A. S. Synthesis and Characterization of a Rhodium(I) σ-Alkane Complex in the Solid State. *Science* **2012,** *337*, 1648.

(34) Pike, S. D.; Krämer, T.; Rees, N. H.; Macgregor, S. A.; Weller, A. S. Stoichiometric and Catalytic Solid–Gas Reactivity of Rhodium Bis-phosphine Complexes. *Organometallics* **2015,** *34*, 1487.

(35) Bloch, W. M.; Burgun, A.; Coghlan, C. J.; Lee, R.; Coote, M. L.; Doonan, C. J.; Sumby, C. J. Capturing snapshots of post-synthetic metallation chemistry in metal-organic frameworks. *Nat. Chem.* **2014,** *6*, 906.

(36) Huxley, M. T.; Young, R. J.; Bloch, W. M.; Champness, N. R.; Sumby, C. J.; Doonan, C. J. Isomer Interconversion Studied through Single-Crystal to Single-Crystal Transformations in a Metal–Organic Framework Matrix. *Organometallics* **2019,** *38*, 3412.

(37) Huxley, M. T.; Burgun, A.; Ghodrati, H.; Coghlan, C. J.; Lemieux, A.; Champness, N. R.; Huang, D. M.; Doonan, C. J.; Sumby, C. J. Protecting-Group-Free Site-Selective Reactions in a Metal-Organic Framework Reaction Vessel. *J. Am. Chem. Soc.* **2018,** *140*, 6416.

(38) Huxley, M. T.; Coghlan, C. J.; Bloch, W. M.; Burgun, A.; Doonan, C. J.; Sumby, C. J. X-ray crystallographic insights into post-synthetic metalation products in a metal-organic framework. *Phil. Trans. R. Soc. A* **2017,** *375*, 20160028.

(39) Burgun, A.; Coghlan, C. J.; Huang, D. M.; Chen, W.; Horike, S.; Kitagawa, S.; Alvino, J. F.; Metha, G. F.; Sumby, C. J.; Doonan, C. J. Mapping-Out Catalytic Processes in a Metal-Organic Framework with Single-Crystal X-ray Crystallography. *Angew. Chem., Int. Ed. Engl.* **2017,** *56*, 1.

(40) Peralta, R.; Huxley, M.; Young, R.; Linder-Patton, O. M.; Evans, J. D.; Doonan, C. J.; Sumby, C. J. MOF Matrix Isolation: Cooperative Conformational Mobility Enables Reliable Single Crystal Transformations. *Faraday Discuss.* **2020,** *DOI: 10.1039/D0FD00012D*.

(41) Spek, T. G.; Scholten, J. J. F. Rh(π-$C_3H_5$)CO($PPh_3$)$_2$ on γ-alumina. Synthesis, texture and infrared spectroscopy. *J. Mol. Cat.* **1977,** *3*, 81.

(42) Sánchez, F.; Iglesias, M.; Corma, A.; del Pino, C. New rhodium complexes anchored on silica and modified Y-zeolite as efficient catalysts for hydrogenation of olefins. *J. Mol. Cat.* **1991,** *70*, 369.

(43) Bernales, V.; Yang, D.; Yu, J.; Gümüşlü, G.; Cramer, C. J.; Gates, B. C.; Gagliardi, L. Molecular Rhodium Complexes Supported on the Metal-Oxide-Like Nodes of Metal Organic Frameworks and on Zeolite HY: Catalysts for Ethylene Hydrogenation and Dimerization. *ACS Appl. Mater. Interfaces* **2017,** *9*, 33511.

(44) Govindasamy, A.; Markova, V. K.; Genest, A.; Rösch, N. Ethene hydrogenation vs. dimerization over a faujasite-supported [Rh($C_2H_4$)$_2$] complex. A computational study of mechanism. *Catal. Sci. Technol.* **2017,** *7*, 102.

(45) Liang, A. J.; Craciun, R.; Chen, M.; Kelly, T. G.; Kletnieks, P. W.; Haw, J. F.; Dixon, D. A.; Gates, B. C. Zeolite-Supported Organorhodium Fragments: Essentially Molecular Surface Chemistry Elucidated with Spectroscopy and Theory. *J. Am. Chem. Soc.* **2009,** *131*, 8460.

(46) Liang, A. J.; Bhirud, V. A.; Ehresmann, J. O.; Kletnieks, P. W.; Haw, J. F.; Gates, B. C. A Site-Isolated Rhodium−Diethylene Complex Supported on Highly Dealuminated Y Zeolite: Synthesis and Characterization. *J. Phys. Chem. B* **2005,** *109*, 24236.

(47) Genna, D. T.; Pfund, L. Y.; Samblanet, D. C.; Wong-Foy, A. G.; Matzger, A. J.; Sanford, M. S. Rhodium Hydrogenation Catalysts Supported in Metal Organic Frameworks: Influence of the

Framework on Catalytic Activity and Selectivity. *ACS Catalysis* **2016,** *6*, 3569.

(48) Evans, J. D.; Sumby, C. J.; Doonan, C. J. Post-synthetic metalation of metal-organic frameworks. *Chem. Soc. Rev.* **2014,** *43*, 5933.

(49) Gonzalez, M. I.; Bloch, E. D.; Mason, J. A.; Teat, S. J.; Long, J. R. Single-crystal-to-single-crystal metalation of a metal-organic framework: a route toward structurally well-defined catalysts. *Inorg. Chem.* **2015,** *54*, 2995.

(50) Bloch, W. M.; Burgun, A.; Doonan, C. J.; Sumby, C. J. Probing post-synthetic metallation in metal-organic frameworks: insights from X-ray crystallography. *Chem. Commun.* **2015,** *51*, 5486.

(51) Banerjee, D.; Kim, S. J.; Parise, J. B. Lithium Based Metal–Organic Framework with Exceptional Stability. *Cryst. Growth Des.* **2009,** *9*, 2500.

(52) Park, K. S.; Ni, Z.; Côté, A. P.; Choi, J. Y.; Huang, R.; Uribe-Romo, F. J.; Chae, H. K.; O'Keeffe, M.; Yaghi, O. M. Exceptional chemical and thermal stability of zeolitic imidazolate frameworks. *Proc. Natl. Acad. Sci.* **2006,** *103*, 10186.

(53) Ibarra, I. A.; Yang, S.; Lin, X.; Blake, A. J.; Rizkallah, P. J.; Nowell, H.; Allan, D. R.; Champness, N. R.; Hubberstey, P.; Schröder, M. Highly porous and robust scandium-based metal–organic frameworks for hydrogen storage. *Chem. Commun.* **2011,** *47*, 8304.

(54) Banerjee, D.; Borkowski, L. A.; Kim, S. J.; Parise, J. B. Synthesis and Structural Characterization of Lithium-Based Metal–Organic Frameworks. *Cryst. Growth Des.* **2009,** *9*, 4922.

(55) Cavka, J. H.; Jakobsen, S.; Olsbye, U.; Guillou, N.; Lamberti, C.; Bordiga, S.; Lillerud, K. P. A New Zirconium Inorganic Building Brick Forming Metal Organic Frameworks with Exceptional Stability. *J. Am. Chem. Soc.* **2008,** *130*, 13850.

(56) Colombo, V.; Galli, S.; Choi, H. J.; Han, G. D.; Maspero, A.; Palmisano, G.; Masciocchi, N.; Long, J. R. High thermal and chemical stability in pyrazolate-bridged metal–organic frameworks with exposed metal sites. *Chem. Sci.* **2011,** *2*, 1311.

(57) DeCoste, J. B.; Peterson, G. W.; Jasuja, H.; Glover, T. G.; Huang, Y.-g.; Walton, K. S. Stability and degradation mechanisms of metal–organic frameworks containing the $Zr_6O_4(OH)_4$ secondary building unit. *J. Mater. Chem. A* **2013,** *1*, 5642.

(58) Wen, L.; Cheng, P.; Lin, W. Solvent-induced single-crystal to single-crystal transformation of a 2D coordination network to a 3D metal–organic framework greatly enhances porosity and hydrogen uptake. *Chem. Commun.* **2012,** *48*, 2846.

(59) Zhang, J.-P.; Liao, P.-Q.; Zhou, H.-L.; Lin, R.-B.; Chen, X.-M. Single-crystal X-ray diffraction studies on structural transformations of porous coordination polymers. *Chem. Soc. Rev.* **2014,** *43*, 5789.

(60) Erdogan, G.; Grotjahn, D. B. Mild and Selective Deuteration and Isomerization of Alkenes by a Bifunctional Catalyst and Deuterium Oxide. *J. Am. Chem. Soc.* **2009,** *131*, 10354.

(61) Kocen, A. L.; Klimovica, K.; Brookhart, M.; Daugulis, O. Alkene Isomerization by "Sandwich" Diimine-Palladium Catalysts. *Organometallics* **2017,** *36*, 787.

(62) Huang, Z.; White, P. S.; Brookhart, M. Ligand exchanges and selective catalytic hydrogenation in molecular single crystals. *Nature* **2010,** *465*, 598.

(63) Yagupsky, M.; Wilkinson, G. Further studies on hydridocarbonyltris(triphenylphosphine)rhodium(I). Part II. Isomerisation of n-pentenes and hex-1-ene. *J. Chem. Soc. A Inorg. Phys. Theor.* **1970,** *1*, 941.

(64) Ballesteros, P.; Lopez, C.; Lopez, C.; Claramunt, R. M.; Jimenez, J. A.; Cano, M.; Heras, J. V.; Pinilla, E.; Monge, A. (2,5-Norbornadiene)rhodium(I) complexes with bis- and tris(azol-1-yl)methanes. *Organometallics* **1994,** *13*, 289.

(65) Robertson, J. J.; Kadziola, A.; Krause, R. A.; Larsen, S. Preparation and characterization of four- and five-coordinate rhodium(I) complexes. Crystal structures of chloro(2-phenylazo)pyridine)(norbornadiene)rhodium(I), (2,2'-bipyridyl)(norbornadiene)rhodium(I) chloride hydrate, and chloro(2,2'-bipyridyl)(norbornadiene)rhodium(I). *Inorg. Chem.* **1989,** *28*, 2097.

(66) Man, B. Y. W.; Bhadbhade, M.; Messerle, B. A. Rhodium(i) complexes bearing N-donor ligands: catalytic activity towards intramolecular cyclization of alkynoic acids and ligand lability. *New J. Chem.* **2011,** *35*, 1730.

(67) Brown, J. M. G., P.J.; Price, D.W. Chirality and the metal-alkene bond; distortions in the soution and solid-state structures of η2-ethene rhodium bis-oxazolinylmethane complexes. *Tetrahedron Asymmetry* **1994,** *5*, 561.

(68) Budzelaar, Peter H. M.; Moonen, Nicolle N. P.; Gelder, René d.; Smits, Jan M. M.; Gal, Anton W. Rhodium and Iridium β-Diiminate Complexes – Olefin Hydrogenation Step by Step. *Eur. J. Inorg. Chem.* **2000,** *2000*, 753.

(69) Young, R. J.; Huxley, M. T.; Pardo, E.; Champness, N. R.; Sumby, C. J.; Doonan, C. J. Isolating reactive metal-based species in Metal–Organic Frameworks – viable strategies and opportunities. *Chem. Sci.* **2020,** *11*, 4031.

(70) Meißner, A.; Preetz, A.; Drexler, H.-J.; Baumann, W.; Spannenberg, A.; König, A.; Heller, D. In Situ Synthesis of Neutral Dinuclear Rhodium Diphosphine Complexes $[\{Rh(diphosphine)(\mu_2\text{-}X)\}_2]$: Systematic Investigations. *ChemPlusChem* **2015,** *80*, 169.

(71) Yang, D.; Odoh, S. O.; Wang, T. C.; Farha, O. K.; Hupp, J. T.; Cramer, C. J.; Gagliardi, L.; Gates, B. C. Metal–Organic Framework Nodes as Nearly Ideal Supports for Molecular Catalysts: NU-1000- and UiO-66-Supported Iridium Complexes. *J. Am. Chem. Soc.* **2015,** *137*, 7391.

(72) Yang, D.; Odoh, S. O.; Borycz, J.; Wang, T. C.; Farha, O. K.; Hupp, J. T.; Cramer, C. J.; Gagliardi, L.; Gates, B. C. Tuning Zr6 Metal–Organic Framework (MOF) Nodes as Catalyst Supports: Site Densities and Electron-Donor Properties Influence Molecular Iridium Complexes as Ethylene Conversion Catalysts. *ACS Catalysis* **2016,** *6*, 235.

(73) Goswami, S.; Noh, H.; Redfern, L. R.; Otake, K.-i.; Kung, C.-W.; Cui, Y.; Chapman, K. W.; Farha, O. K.; Hupp, J. T. Pore-Templated Growth of Catalytically Active Gold Nanoparticles within a Metal–Organic Framework. *Chemistry of Materials* **2019,** *31*.

(74) Schrock, R. R.; Osborn, J. A. Catalytic hydrogenation using cationic rhodium complexes. I. Evolution of the catalytic system and the hydrogenation of olefins. *J. Am. Chem. Soc.* **1976,** *98*, 2134.

(75) Iglesias, M.; Del Pino, C.; Corma, A.; Garcia-Blanco, S.; Martinez Carrera, S. Rhodium complexes with phosphine and diazabutadiene ligands. Their properties as hydrogenation catalysts. Molecular structure of $RhCl(COD)P(p\text{-}C_6H_4F)_3$. *Inorg. Chim. Acta* **1987,** *127*, 215.

(76) Preetz, A.; Drexler, H.-J.; Fischer, C.; Dai, Z.; Börner, A.; Baumann, W.; Spannenberg, A.; Thede, R.; Heller, D. Rhodium-Complex-Catalyzed Asymmetric Hydrogenation: Transformation of Precatalysts into Active Species. *Chem. Eur. J.* **2008,** *14*, 1445.

(77) Smidt, S. P.; Zimmermann, N.; Studer, M.; Pfaltz, A. Enantioselective hydrogenation of alkenes with iridium-PHOX catalysts: a kinetic study of anion effects. *Chem. Eur. J.* **2004,** *10*, 4685.

(78) Chen, J.; Wang, J.; Guo, L.; Li, L.; Yang, Q.; Zhang, Z.; Yang, Y.; Bao, Z.; Ren, Q. Adsorptive Separation of Geometric Isomers of 2-Butene on Gallate-Based Metal–Organic Frameworks. *ACS Appl. Mater. Interfaces* **2020,** *12*, 9609.

(79) Kanai, H.; Choe, S. B.; Klabunde, K. J. Isomerization of 1-butene catalyzed by (.eta.6-arene)NiR2. A very active homogeneous catalyst system. *J. Am.Chem. Soc.* **1986,** *108*.

(80) Tolman, C. A. Chemistry of tetrakis(triethyl phosphite)nickel hydride, HNi[P(OEt)3]4+. IV. Mechanism of olefin isomerization. *J. Am.Chem. Soc.* **1972,** *94*.

(81) Sen, A.; Lai, T. W. Mechanism of palladium(II)-catalyzed

carbon-carbon double bond isomerization in olefins. *Inorganic Chemistry* **1984,** *23*.

(82) Xiao, D. J.; Oktawiec, J.; Milner, P. J.; Long, J. R. Pore Environment Effects on Catalytic Cyclohexane Oxidation in Expanded $Fe_2$(dobdc) Analogues. *J. Am. Chem. Soc.* **2016,** *138*, 14371.

(83) Willems, T. F.; Rycroft, C. H.; Kazi, M.; Meza, J. C.; Haranczyk, M. Algorithms and tools for high-throughput geometry-based analysis of crystalline porous materials. *Micropor. Mesopor. Mat.* **2012,** *149*, 134.

(84) Ongari, D.; Boyd, P. G.; Barthel, S.; Witman, M.; Haranczyk, M.; Smit, B. Accurate Characterization of the Pore Volume in Microporous Crystalline Materials. *Langmuir* **2017,** *33*, 14529.

(85) Becke, A. D. Density-functional exchange-energy approximation with correct asymptotic behavior. *Phys. Rev. A* **1988,** *38*, 3098.

(86) Perdew, J. P. Density-functional approximation for the correlation energy of the inhomogeneous electron gas. *Phys. Rev. B* **1986,** *33*, 8822.

(87) Neese, F. The ORCA program system. *WIREs Comp. Mol. Sci.* **2012,** *2*, 73.

(88) Neese, F. Software update: the ORCA program system, version 4.0. *WIREs Comp. Mol. Sci.* **2018,** *8*, e1327.

(89) Neese, F.; Wennmohs, F.; Hansen, A.; Becker, U. Efficient, approximate and parallel Hartree–Fock and hybrid DFT calculations. A 'chain-of-spheres' algorithm for the Hartree–Fock exchange. *Chem. Phys.* **2009,** *356*, 98.

(90) Weigend, F.; Ahlrichs, R. Balanced basis sets of split valence, triple zeta valence and quadruple zeta valence quality for H to Rn: Design and assessment of accuracy. *Phys. Chem. Chem. Phys.* **2005,** *7*, 3297.

(91) Weigend, F. Accurate Coulomb-fitting basis sets for H to Rn. *Phys. Chem. Chem. Phys.* **2006,** *8*, 1057.

(92) Grimme, S.; Ehrlich, S.; Goerigk, L. Effect of the damping function in dispersion corrected density functional theory. *J. Comput. Chem.* **2011,** *32*, 1456.

(93) Henkelman, G.; Jónsson, H. Improved tangent estimate in the nudged elastic band method for finding minimum energy paths and saddle points. *J. Chem. Phys.* **2000,** *113*, 9978.

(94) Dubbeldam, D.; Calero, S.; Ellis, D. E.; Snurr, R. Q. RASPA: molecular simulation software for adsorption and diffusion in flexible nanoporous materials. *Mol Simul.* **2016,** *42*, 81.

(95) Wick, C. D.; Martin, M. G.; Siepmann, J. I. Transferable Potentials for Phase Equilibria. 4. United-Atom Description of Linear and Branched Alkenes and Alkylbenzenes. *J. Phys. Chem. B* **2000,** *104*, 8008.

(96) Rappe, A. K.; Casewit, C. J.; Colwell, K. S.; Goddard, W. A.; Skiff, W. M. UFF, a full periodic table force field for molecular mechanics and molecular dynamics simulations. *J. Am. Chem. Soc.* **1992,** *114*, 10024.

TOC Figure: